Lithium niobate *X*-cut, *Y*-cut, and *Z*-cut surfaces from *ab initio* theory

Simone Sanna* and Wolf Gero Schmidt
Lehrstuhl für Theoretische Physik, Universität Paderborn, 33095 Paderborn, Germany
(Received 1 March 2010; revised manuscript received 4 May 2010; published 21 June 2010)

Density-functional theory calculations of the $LiNbO_3$ $(2\bar{1}\bar{1}0)$, $(1\bar{1}00)$, and (0001) surfaces, commonly referred to as *X*, *Y*, and *Z* cuts, are presented. In case of the *Z* cut, we find a pronounced dependence of the surface structure and stoichiometry on the direction of the ferroelectric polarization. In contrast, the influence of the chemical potentials of the surface constituents is limited. Rather electrostatics governs the surface stability. Different from the *Z* cut, the stoichiometry of the *X* cut and *Y* cut is clearly dependent on the preparation conditions. The surface charge observed for the nominal nonpolar *Y* cut is traced back to the formation of a strong surface dipole.

DOI: 10.1103/PhysRevB.81.214116 PACS number(s): 68.35.Md, 82.65.+r, 77.84.Ek

I. INTRODUCTION

Lithium niobate (LN) is a ferroelectric material frequently used for various (nonlinear) optical and acoustic applications.[1,2] Due to its unusually pronounced piezoelectric, pyroelectric, and photorefractive properties,[3] LN has been used for the realization of surface acoustic wave devices, electro-optical modulators, and holographic recording.[4] While traditional applications mainly exploit LN bulk properties, more recently the (microscopic) surface and interface properties have become important. Periodically poled LN structures[5] and substrate-assisted self-assembly of nanostructures[6] are examples of the emerging applications. Furthermore, LN has attracted a lot of attention as a substrate for the GaN growth, either for the realization of monolithic optoelectronic amplifiers[7–9] or as an alternative substrate (to α-Al_2O_3) for the quasilattice matched growth of GaN.[10–13]

The microscopic understanding of LN surfaces is comparatively poor, however. This is due in part to the lack of surface analysis studies performed in ultrahigh vacuum and in part to the nature of the material itself. The surface properties of ferroelectrics such as LN are controlled both by the direction of the spontaneous polarization and by the growth conditions. The subtle balance between the ionic and covalent character of the metal-oxygen bonds can be affected by small temperature changes during the growth, resulting in an inversion of the polarization direction.[14] Among the technologically relevant surfaces, the LN *Z* cut is most intensively investigated, both from experiment[15–18] as well as *ab initio* theory.[19,20] Density-functional theory (DFT) investigations predict stoichiometric differences between positive and negative surfaces. Low-energy electron diffraction and reflection high-energy electron diffraction (LEED/RHEED) did not indicate any reconstruction of either the positive and or the negative surface[15] and UV-photoelectron emission microscopy (PEEM) found the ionization energy of the two surfaces to differ by about 2 eV.[16] LN *Z* cuts can be made atomically smooth by a temperature treatment.[17] However, annealing the samples in vacuum can lead to the evaporation of different Li and O gases depending on the annealing temperature, as revealed by Auger electron spectroscopy and mass spectrometry.[18] Lithium niobate *X* cuts and *Y* cuts are also of technological relevance[21] and some information regarding growth techniques and postgrowth treatments (to improve the sample quality) can be found.[22] However, little detailed information on the surface atomic structure is available.

The present study aims at the microscopic understanding of clean *X*-cut, *Y*-cut, and *Z*-cut lithium niobate. For this end, we perform total-energy calculations within DFT and construct surface phase diagrams in dependence on the chemical potentials of the surface constituents. The stoichiometry of the *Z*-cut surfaces are found to differ from a bulk-terminated face. They are characterized by different terminations and morphology, with the positive surface containing more Li and O than the negative surface. The termination of the nonpolar *X* cut depends on the growth conditions. Among the stable terminations, the nonstoichiometric play a prominent role, in contrast to the *Y* cut.

In the following, we introduce the LN crystal structure and the common notation of crystal faces. Thereafter the computational methodology is described before we present and discuss the numerical results.

II. PLANES AND FACES

LN is a complex bimetallic oxide with spontaneous ferroelectric polarization directed along the [0001] direction. LN becomes paraelectric only at 1483 K, which makes this phase not particularly relevant for technical applications. Therefore, we will exclusively discuss the surfaces of the ferroelectric phase.

Ferroelectric LN exhibits threefold rotational symmetry about its *c* axis and three mirror planes. It is therefore a trigonal material belonging to the 3*m* point group (space group *R*3*c*). The LN structure above the ferroelectric Curie temperature consists of planar sheets of LiO_3 and Nb atoms piled along the *c* axis. The Nb atoms (nominal valence state +5) are centered between the oxygen layers (the nominal valence state of each oxygen atom is −2 and the nominal valence state of Li is +1) and the material is nonpolar (Fig. 1). Below Curie temperature, the elastic forces of the crystal dominate and force Nb and Li ions to leave their positions. This yields to a different ordering of the atomic sheets, which becomes, in the +*c* direction, Nb-O_3-Li, Nb-O_3-Li, …, as shown in Fig. 1(a). The charge separation resulting from

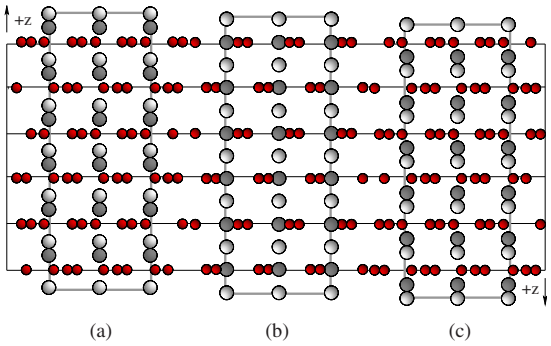

FIG. 1. (Color online) Stacking sequence of the atoms in the ferroelectric phase ($T<T_C$) of lithium niobate (a) and (c) and in the high-symmetry paraelectric phase ($T\geq T_C$) (b) of LN. The displacement of the cations due to the ferroelectric phase transition and the two possible domain directions are indicated.

this shift makes the material polar (displacement ferroelectrics). The spontaneous polarization (0.7 C/m^2) is unusually high[4] and directed along the c axis. Cutting the material perpendicularly to this direction will result in the creation of two differently polarized (0001) surfaces with peculiar properties such as macroscopic polarization charge.

Crystals belonging to the trigonal may be represented by a rhombohedral or by a hexagonal unit cell, with several possibilities for the choice of the primitive vectors. The cells used in this work are shown in Fig. 2. The conventional rhombohedral unit cell contains two formula weights (10 atoms) while the conventional hexagonal unit cells contains six formula weights (30 atoms). The coordinate system used to describe the physical properties of LN is, however, neither rhombohedral nor hexagonal but a Cartesian x, y, and z system. In fact, many physical properties and symmetries of the

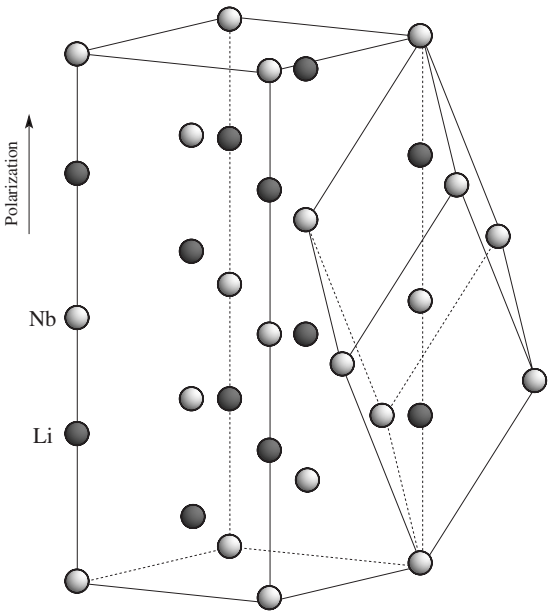

FIG. 2. Conventional rhombohedral unit cell and conventional hexagonal unit cell of ferroelectric $LiNbO_3$. Li atoms are gray and Nb atoms are white. For the sake of clarity, the oxygen atoms are omitted.

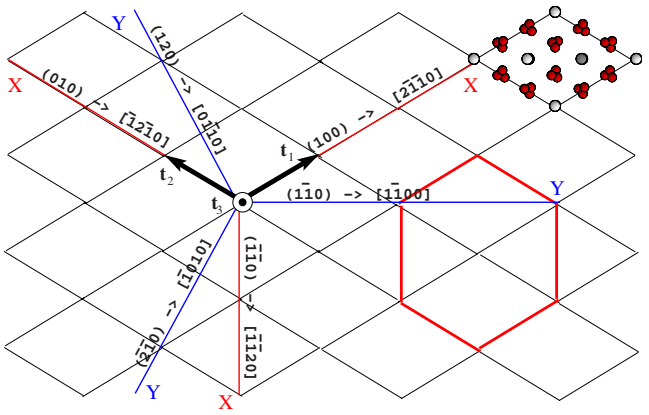

FIG. 3. (Color online) Relationships between the conventional hexagonal coordinate system and the Cartesian coordinate system used in this work (real-space representation). X and Y label the x direction and y direction, $\boldsymbol{t_1}$, $\boldsymbol{t_2}$, and $\boldsymbol{t_3}$ are the translational basis vectors of the hexagonal lattice. In round brackets the (real-space) vectors expressed in terms of the basis $\boldsymbol{t_1}$, $\boldsymbol{t_2}$, and $\boldsymbol{t_3}$, and in square brackets the corresponding Miller-Bravais indices indicating the crystallographic directions.

material are conveniently described in this coordinate system. The most widely used coordinate systems are the orthohexagonal and the pseudocubic rhombohedral systems, which are described in Ref. 23. The presence of different notations and the fact that the conventions are not always obeyed generates some confusion. We follow Ref. 3 in the definition of the LN X, Y, and Z cuts, which is shortly summarized in the following. In Fig. 3, we show the hexagonal lattice with the standard basis vectors $\boldsymbol{t_1}$, $\boldsymbol{t_2}$, and $\boldsymbol{t_3}$. According to Ref. 3, the z axis is parallel to the crystal c axis. The x axis coincides with one of the three equivalent translation vectors of the conventional hexagonal unit cell. These have, in the real-space representation, the directions of the three vectors (100), (010), and ($1\bar{1}0$). Using the conversion formula,

$$(u,v,w) \rightarrow [2u-v,-u+2v,-u-v,3w]$$

they correspond to the crystallographic directions [$2\bar{1}\bar{1}0$], [$\bar{1}2\bar{1}0$], and [$\bar{1}\bar{1}20$], as shown in Fig. 3. Once the x axis and the z axis are determined, the y axis is chosen to be orthogonal and right handed. This means that the y axis will have the direction of the real-space vectors ($1\bar{1}0$), (120), and ($\bar{2}10$) and crystallographic directions [$1\bar{1}00$], [$01\bar{1}0$], and [$\bar{1}010$], i.e., the y axis lies in a plane of mirror symmetry. Following the standard convention, the LN X cut, Y cut and Z cut are the planes normal to the x, y, and z axes and are characterized by the Miller-Bravais indices ($2\bar{1}\bar{1}0$), ($1\bar{1}00$), and (0001), respectively, as shown in Figs. 3 and 4.

The Z cut is perpendicular to the spontaneous polarization of the material and is therefore a polar plane, with a nominal surface charge $\sigma_0^z=0.7$ C/m^2. The measured surface charge σ^z is however three order of magnitude smaller,[24] indicating that charge compensation mechanisms occur at the surface.

The X and Y cuts are nominally nonpolar. The Y cut, however, shows a surface charge σ^y as big as one third of

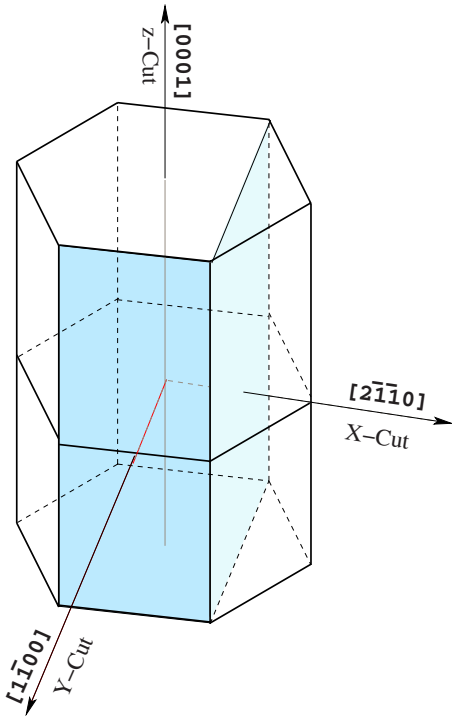

FIG. 4. (Color online) Real-space representation of the x axis, y axis, z axis and of the X cut and Y cut as defined and used in this work.

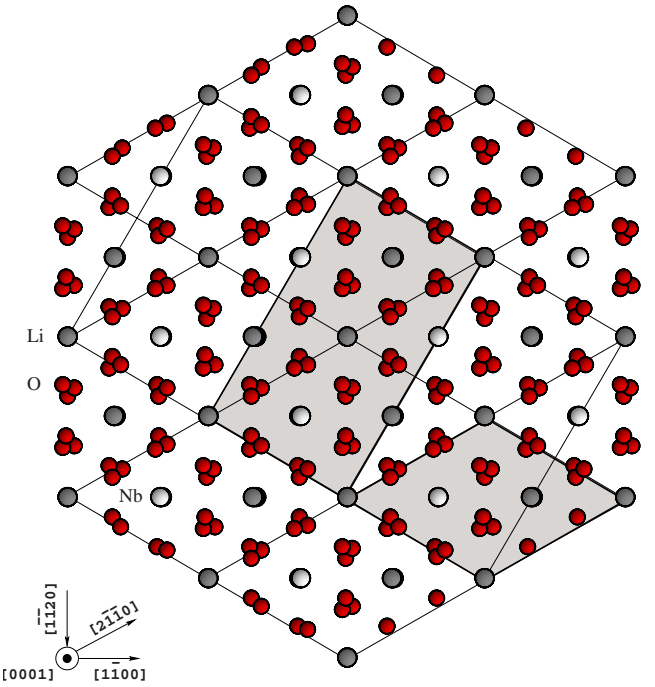

FIG. 5. (Color online) Top view of the two supercells used to model the LN slabs. The orthogonal supercell is in the middle of the picture and the hexagonal supercell on the lower right corner.

σ^z.[25] Furthermore, σ^y changes upon compression in the y direction (piezoelectricity). This is not the case for the X cut because the x axis is perpendicular to a mirror plane and any charge movement on one side of the plane is mirrored on the opposite site.

III. METHODOLOGY

Our first-principles calculations within the DFT use the all-electron projector-augmented wave method[26] as implemented in VASP.[27] The PW91 formulation of the generalized gradient approximation (GGA) exchange-correlation functional,[28] plane-wave expansions up to 400 eV, and projectors up to $l=3$ for Nb and $l=2$ for Li and O have been used for the calculations. This approach yields reliable structures and energies for bulk LN in the ferroelectric and paraelectric phase.[29] As there is no experimental evidence of LN surfaces with net spin moment, we restrict ourself to spin-unpolarized calculations. The dipole corrections described in Refs. 30 and 31 have been used to correct the spurious interactions due to the slab periodic images.

A. Computational

The slabs for the simulation of (0001) surfaces are hexagonal supercells based on the hexagonal unit cell shown in Fig. 2 consisting of 12 Nb-O_3-Li trilayers (60 atoms) plus a surface termination and a vacuum layer of ≈15 Å. The outer three trilayers (i.e., nine LN layers) and all the termination atoms are allowed to relax freely (force threshold 0.02 eV/Å) while the remaining layers are kept fixed to simulate the bulk of the material. As no other surface periodicity than the 1×1 has been observed for both the positive and the negative Z cuts,[15] we do not consider surface reconstructions.

Neither the hexagonal nor the rhombohedral unit cell shown in Fig. 2 is appropriate for the simulation of the LN X cut and Y cut, as none of the cell faces is parallel to the LN cut. For this reason, we define a different unit cell, with all the axes orthogonal and of different length. The new unit cell has the same height of the hexagonal unit cell but twice its volume. The cell contains 12 formula weights (60 atoms) and is depicted in Fig. 5. Based on this unit cell, the slabs for the simulation of the X cut and of the Y cut are set up.

For the simulation of the X cut, we double the orthogonal unit cell along the x direction, so that the slab consists of a stacking in the x direction of four Li_6Nb_6-O_9-O_9 trilayers (120 atoms) plus a surface termination and ≈15 Å of vacuum. The atomic positions of the first nine layers have been fixed at bulk values. The outer three layers and all of the terminating atoms in the slab unit cell are allowed to relax freely.

For the simulation of the Y cut, we double the new unit cell along the y direction so the slab consists of 12 $Li_2Nb_2O_6$ layers (120 atoms) plus a surface termination and ≈18 Å of vacuum. The last four $Li_2Nb_2O_6$ layers and all the terminations atoms are allowed to relax while the rest is frozen at the bulk positions. A Monkhorst-Pack[32] k-point mesh was used to carry out the integration in the Brillouin zone for the simulation of the X cut, Y cut, and Z cut. In order to reflect the geometry of the supercell, our meshes consist of a single k point in the direction perpendicular to the surface and 2×2 k points in the remaining directions. The convergence of the k-point mesh has been tested with respect to total-energy

differences, band structure, atomic forces, and ionization energy.

B. Surface energetics

To compare energetically LN surfaces with different stoichiometry, we follow Refs. 33–35 and use the grand (or Landau) potential Ω, approximated as

$$\Omega(\mu_{\mathrm{Li}},\mu_{\mathrm{Nb}},\mu_{\mathrm{O}}) \approx E^{\mathrm{DFT}}(N_{\mathrm{Li}},N_{\mathrm{Nb}},N_{\mathrm{O}}) - \sum_{i}^{\mathrm{Li,Nb,O}} \mu_i N_i. \quad (1)$$

Here $E^{\mathrm{DFT}}(N_{\mathrm{Li}},N_{\mathrm{Nb}},N_{\mathrm{O}})$ is the total energy calculated within DFT for the respective slab containing N_{Li} Li atoms, N_{Nb} Nb atoms, and N_{O} O atoms and μ_{Li}, μ_{Nb}, and μ_{O} are the chemical potentials of Li, Nb, and O determined by the experimental conditions. Equation (1) is not an equality and holds only in approximate form, as the surface free energy ($F_s=U_s-TS_s$ with U_s being the internal energy) should be used rather than the DFT total energy. However, it must be considered that (1) the direct influence of the pressure variation on the surface energy can be neglected, (2) the contribution of the surface formation entropy S_s to the surface energy at a certain temperature is similar for the different surfaces we want to compare, and (3) a wide compensation of the lattice-dynamical contributions to F_s is expected. Consequently, the free energy can nearly be replaced by the total energy E. Furthermore, as one expects a compensation of the effects of the zero-point vibrations on the total energy and on the chemical potentials, the total energy E is usually replaced by the DFT total energy E^{DFT} in explicit calculations.[35]

For convenience, we use in the following the chemical-potential variations:

$$\Delta\mu_{\mathrm{Li}} = \mu_{\mathrm{Li}} - \mu_{\mathrm{Li}}^{\mathrm{bulk}},$$

$$\Delta\mu_{\mathrm{Nb}} = \mu_{\mathrm{Nb}} - \mu_{\mathrm{Nb}}^{\mathrm{bulk}},$$

$$\Delta\mu_{\mathrm{O}} = \mu_{\mathrm{O}} - \frac{1}{2}\mu_{\mathrm{O}_2}^{\mathrm{gas}} \quad (2)$$

as variables, the thermodynamically allowed range of which is restricted by several conditions, see also Ref. 36.

From the definition of the LN heat of formation, it follows

$$\Delta H_f^{\mathrm{LN}} = \mu_{\mathrm{LN}} - \mu_{\mathrm{Li}} - \mu_{\mathrm{Nb}} - 3\mu_{\mathrm{O}}. \quad (3)$$

Given that upper limits are given by the respective bulk phases, the variables are bound within

$$\Delta H_f^{\mathrm{LN}} \leq \Delta\mu_i \leq 0 \quad i = \mathrm{Li,Nb,O}. \quad (4)$$

Thus, the variation in each μ_i is constrained in a range given by ΔH_f^{LN} below its bulk value. The i-rich preparation conditions are given by $\Delta\mu_i=0$.

Equation (1) can be simplified considering that only two of three chemical potentials are linearly independent,

$$\mu_{\mathrm{Li}} + \mu_{\mathrm{Nb}} + 3\mu_{\mathrm{O}} = \mu_{\mathrm{LN}}^{\mathrm{bulk}}.$$

We express μ_{Nb} as a function of μ_{Li} and μ_{O} since the latter can be better controlled experimentally. Furthermore, with this choice our results are directly comparable with earlier calculations for the Z cut.[19] It follows

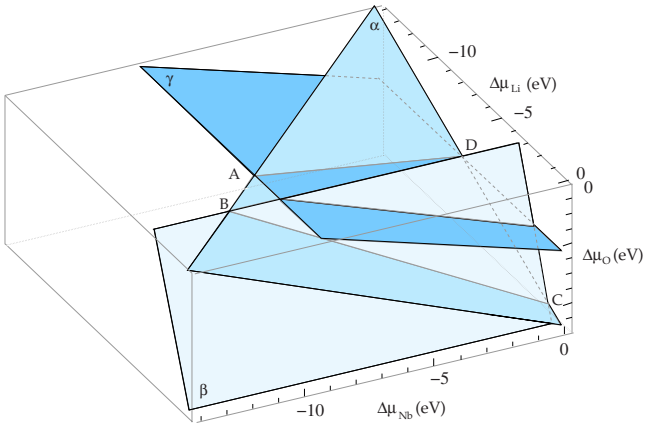

FIG. 6. (Color online) Stability range of $\Delta\mu_{\mathrm{Li}}$, $\Delta\mu_{\mathrm{Nb}}$, and $\Delta\mu_{\mathrm{O}}$. Only within the region ABCD LN surfaces are formed.

$$\Omega(\Delta\mu_{\mathrm{Li}},\Delta\mu_{\mathrm{O}}) = E(N_{\mathrm{Li}},N_{\mathrm{Nb}},N_{\mathrm{O}}) - \Delta\mu_{\mathrm{Li}}(N_{\mathrm{Li}}-N_{\mathrm{Nb}}) - \Delta\mu_{\mathrm{O}}(N_{\mathrm{O}}-3N_{\mathrm{Nb}}) - \mu_{\mathrm{Li}}^{\mathrm{bulk}}(N_{\mathrm{Li}}-N_{\mathrm{Nb}}) - \frac{1}{2}\mu_{\mathrm{O}_2}^{\mathrm{gas}}(N_{\mathrm{O}}-3N_{\mathrm{Nb}}) - N_{\mathrm{Nb}}\mu_{\mathrm{LN}}^{\mathrm{bulk}}. \quad (5)$$

The values of the bulk chemical potentials are approximated by the total energy per atom calculated within DFT. The total energies of bulk Li and Nb, oxygen gas, Li_2O, Nb_2O_5, and $LiNbO_3$ have been calculated with the approach described in Sec. III A, using in each case their primitive cells and minimizing the respective lattice constants. The gas phase of oxygen has been calculated with an oxygen dimer in a vacuum box of sides 10 Å. No correction for the known GGA overbinding problem is considered,[37] as it would not qualitatively change any of the conclusions of this work. Metallic Li and metallic Nb both crystallize at high temperatures (i.e., above room temperature) in the body-centered-cubic structure (space group $Im\bar{3}m$).[38] Lithium oxide (LO) has, like many oxides of univalent ions the antifluorite arrangement (space group $Fm\bar{3}m$) shown in Ref. 38. There are different niobium oxides (NO), among them niobium pentoxide (Nb_2O_5) is the most stable at high temperatures.[39] Nb_2O_5 itself occurs in several modifications, whose number and nature is still not certain. Most of the known polytypes have a complicate crystal structure with long-range ordering. To calculate the formation enthalpy of NO, we use therefore the R-Nb_2O_5 phase, which is not the stable phase at high temperatures, but is the only phase for which complete structural information is available.[36] This results in an uncertainty in the position of the line AD of Fig. 6, increasing or decreasing the stability range of the LN surfaces by an amount which is difficult to quantify. However, the cohesive energies of different polytypes is rarely bigger than of a few electron volt tenths, as long as we consider solid phases.[35]

The heat of formation of LN, LO, and NO have been calculated as the difference between the total energy of the

TABLE I. Total energy per formula unit and heat of formation of relevant compounds (in eV). Besides the calculated values (a), the measured values (Exp.) and the results of earlier calculations (Ref. 36) (b) are reported for comparison.

System	Theory (a)	Theory (b)	Exp.
$LiNbO_3$	−39.814	−39.552	
Li_2O	−14.436	−14.461	
Nb_2O_5	−62.434	−60.319	
Li	−1.893	−1.895	
Nb	−10.064	−10.049	
O_2	−4.411	−4.392	
$\Delta H_f[LiNbO_3]$	−14.624	−14.433	−14.149[a]
$\Delta H_f[Li_2O]$	−6.239	−6.280	−6.230[b]
$\Delta H_f[Nb_2O_5]$	−20.251	−18.262	−19.775[b]

[a]Reference 40.
[b]Reference 41.

compounds and the composition-weighted sum of their constituents,

$$\Delta H_f^{AB} = E_{AB}^{bulk} - E_A^{bulk} - E_B^{bulk}. \quad (6)$$

The DFT-GGA calculations tend to overestimate the experimental value. However, even for the largest deviation from experiment (in the case of LN), the overestimation is only about 3%, in agreement with earlier calculations.[36] Our results are compiled in Table I and compared with literature data. We observe a general agreement with previous calculations, a part from a noticeable difference in the NO total energy, which might be due to different computational parameters. If the surface is in equilibrium with the bulk substrate, Li, Nb, and O atoms can be exchanged with the bulk. The equilibrium condition,

$$\Delta H_f^{LN} = \Delta\mu_{Li} + \Delta\mu_{Nb} + 3\Delta\mu_O \quad (7)$$

represents a plane in a three-dimensional space (denoted as α in Fig. 6) whose axes represent the chemical-potential variations in Li, Nb, and O. Only within this plane, LN surfaces are thermodynamically stable. However, further constraints have to be considered. Stability against the formation of LO and NO requires

$$2\Delta\mu_{Li} + \Delta\mu_O \leq \Delta H_f^{LO} \quad (8)$$

and

$$2\Delta\mu_{Nb} + 5\Delta\mu_O \leq \Delta H_f^{NO}. \quad (9)$$

These conditions are represented by the planes β and γ in Fig. 6. The regions above the planes β and γ represent growth conditions at which the oxides are formed. Beyond these values new bulk phases (either Li and Nb oxides or the bulk phases of Li, Nb, and O) will start to precipitate on the LN surfaces. Only within the region ABCD in Fig. 6 LN surfaces are stable. This region will be indicated in the phase diagrams discussed below.

IV. RESULTS

A. Z Cut

Even if the LN *Z* cut is the most relevant surfaces for applications, only few experimental studies of the LN (0001) surface structure are available.[15,18,42,43] Besides the 1×1 surface periodicity revealed by LEED/RHEED investigations,[15] we know from mass-spectrometric investigations that upon annealing in vacuum at different temperatures different evaporation regimes are observed. In particular, the evaporation of LiO from the positive surface is one order of magnitude larger than from the negative surface and the evaporation of Li and O_2 gases from the negative surface is almost negligible.[18] This was attributed to a reduction process which equilibrates the oxygen concentration between the crystal and the environment thereby removing oxygen from the bulk to replace the desorbed species from the surface. Annealing is often done in order to clean the surface from adsorbed ambient species and obtain an atomically flat surface as required in many applications.[17] The evaporation of different species at different temperature explains why in some experiment the LN surface appears to be predominantly oxygen terminated[15] while in other, it seems to be terminated with an Nb atomic layer.[44]

We investigate the relative stability of different surface structure candidates, represented by stoichiometric and nonstoichiometric surface terminations with different morphology. The different terminations have been chosen following the approach described in Ref. 19. We consider -Nb-O_x-Li_y as positive termination and -Li_j-O_i as negative surface termination, whereby $x=1,2,3,4$, $y=0,1,2$, $i=0,1,2,3$, and $j=0,1$. All the possible combinations in different starting geometries of each termination have been investigated, resulting in the simulation of more than 80 different slabs. In this way all the possible bulk cuts as well as nonstoichiometric surfaces are modeled.

Evaluating the formation energy of the candidate terminations [given in the grand potential by Eq. (5)] at each point $P(\Delta\mu_O, \Delta\mu_{Li})$, we are able to draw the phase diagrams of the positive and negative LN (0001) surfaces shown in Fig. 7. The differently polarized surfaces differ clearly in their stoichiometry, showing that the intrinsic polarization plays an important role in the surface stabilization. In general, the terminations of the positive surface contain more oxygen than those of the negative surface under the same conditions. Within the thermodynamically allowed range (indicated in the plot), the stable termination for the positive surface is -Nb-O_3-Li_2 while for the negative surface, the O-Li termination is favored under most condition. Under O-rich conditions, the surface can become O_2 or O_3 terminated. This is in fairly good agreement with Ref. 19. All the occurring terminations are nonstoichiometric, i.e., LN polar surfaces vary their stoichiometry to reduce the surface energy. Ion scattering spectroscopy (ISS) measurements have shown recently that both the positive and the negatively poled surfaces are predominantly oxygen terminated.[15] Considering that ISS is largely insensitive to Li because of its low atomic number and mass, our results confirm the experimental observations.

The relaxed atomic structure of the preferred terminations for the positive and negative surface is shown in Fig. 8.

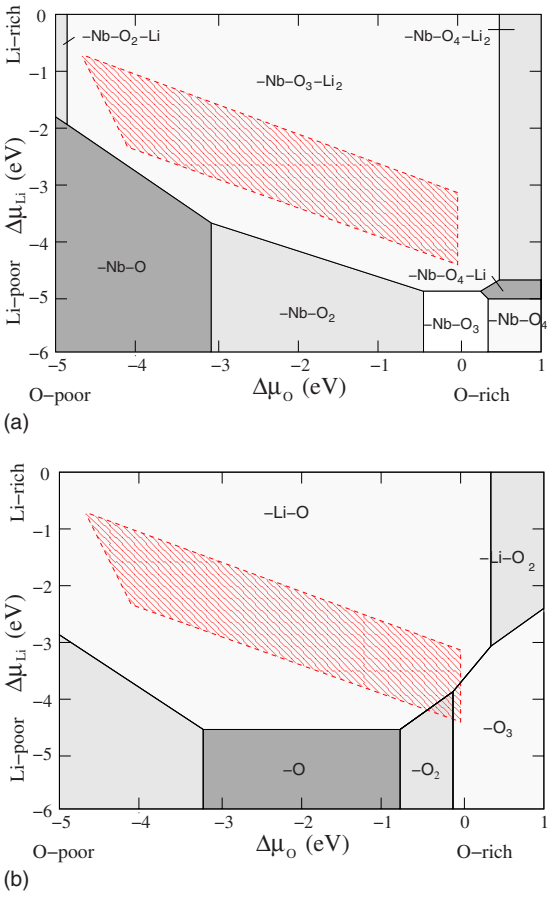

FIG. 7. (Color online) Phase diagram of the positive (upper part) and negative (lower part) LN (0001) surface at different growth conditions and in absence of foreign adsorbates. The unlabeled region corresponds to the Nb-terminated bulk cut. The shaded region indicates the thermodynamically range of the chemical potentials.

While the negative surface does not show any change in the succession of the atomic planes stapled along the [0001] direction with respect to the bulk, the positive surface is characterized by the relaxation of one Li into the lower laying oxygen plane, as shown in Fig. 9. The atomic relaxation is otherwise not pronounced, involves in both cases only the

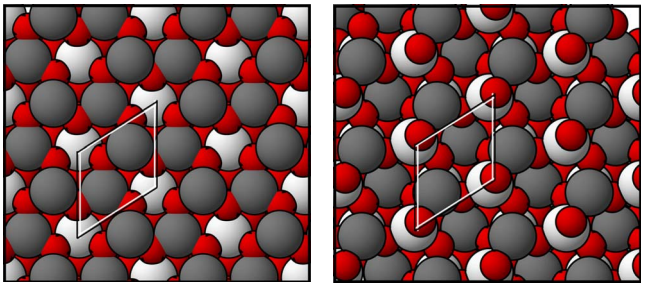

FIG. 8. (Color online) Space-fill models of the stable positive (-Nb-O_3-Li_2 terminated, left-hand side) and negative (O-Li- terminated, right-hand side) LN (0001) surface at growth conditions. White atoms are Nb, gray atoms Li, and small atoms O. The surface unit cell is outlined.

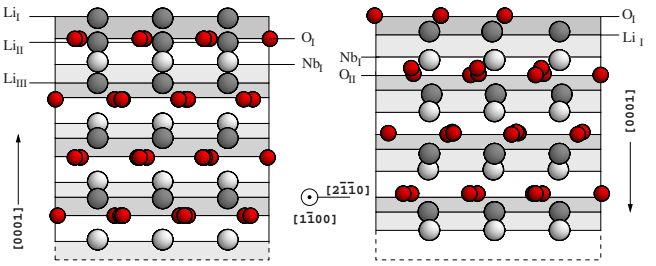

FIG. 9. (Color online) Side view of the stable positive (-Nb-O_3-Li_2 terminated) and negative (O-Li- terminated) LN (0001) surface. White atoms are Nb, gray atoms Li, and small atoms O.

two outer trilayers and consists mainly in an outward relaxation of the cationic layers. The distances between the atomic layers are reported in Table II.

Both the stable -Nb-O_3-Li_2 termination of the positive surface and the O-Li termination of the negative surface are found to be semiconducting. In Fig. 10, we show the density of states (DOS) calculated for bulk LN, and the partial DOS of the last three LN trilayers (including the surface terminations) of the slabs used for the simulation of the two surfaces. The latter have been calculated correcting for the potential variation within the slabs. The DOS of bulk and surface slabs show only minor differences, indicating that the presence of the surfaces does not change significantly the LN band gap.

The phase diagram does not only contain information about the stable surface terminations but is also useful to interpret the results of experimental investigations. When the values of the chemical potentials decrease, both the stable positive surface -Nb-O_3-Li_2 and the stable negative surface O-Li-lose Li and O and become -Nb-O and Nb terminated, respectively, as shown in Fig. 7. No Nb loss is expected according to our calculations. This explains why evaporation of Li, O_2, and LiO but not of Nb was observed (if not close to the Curie temperature) from the positive and negative surfaces.[18] This also explains why coaxial-impact collision ion scattering spectroscopy studies find the surface after thermal treatment to be terminated by a Nb atomic layer (in

TABLE II. Distances between the atomic layers of the stable Z surfaces. Corresponding bulk values are reported for comparison, all lengths in angstrom.

	Surf.	Bulk
	Z^+	
$d(Li_I, O_I)$	0.78	
$d(Li_{II}, O_I)$	0.14	
$d(Li_{III}, Nb_I)$	0.89	0.65
$d(Nb_I, O_I)$	0.89	0.98
	Z^-	
$d(O_I, O_{II})$	2.34	2.31
$d(O_I, Li_I)$	0.63	0.68
$d(Li_I, Nb_I)$	1.11	0.66
$d(Nb_I, O_I)$	1.74	1.33

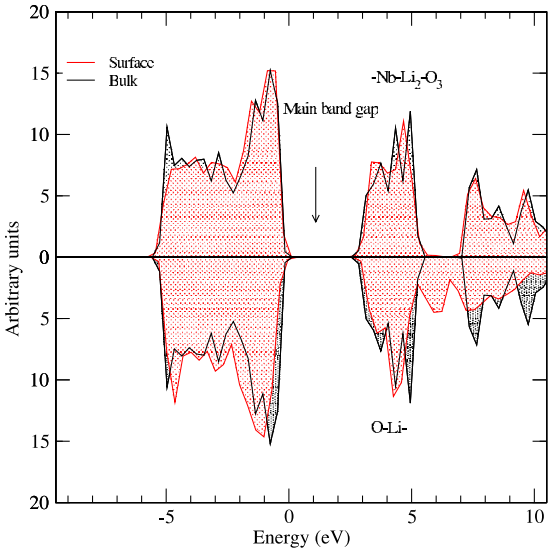

FIG. 10. (Color online) Partial density of states (DOS) of the last three LN trilayers of the slab used to simulate the stable positive (upper part) and negative (lower part) LN (0001) surface. The bulk DOS is reported for comparison. Neither the positive nor the negative termination drastically changes the fundamental band gap. The zero of the energy scale is the LN valence-band maximum.

which the Nb atoms are not shifted from the bulk positions).[44] In the cited experiment, no attempt to distinguish between positively and negatively poled surfaces has been done. According to our phase diagrams, the transition from -Nb-O_3-Li_2 to -Nb-O occurs at the positive surface at higher values of the chemical potentials (i.e., at lower temperatures) than the transition from O-Li- to Nb- for the negative surfaces. This explains why the observed evaporation of LiO from the positive surface was an order of magnitude larger than the evaporation from the negative surface[18] and is in very good agreement with the calculations of Ref. 19. To further characterize the LN *Z* cut, the electronic ionization energy (W^+, W^-) of the two surfaces has been calculated (see Table III), following the approach described in Ref. 45. As shown in Fig. 11, the ionization energy *W* for a semiconductor is defined as the sum of the band-gap energy E_g and of the electron affinity χ, which is, on turn, a function of the surface dipole induced by various surface effects such as surface termination, reconstruction, atomic steps, and adsorbates. The calculated values of $W^+=6.5$ eV for the positive surface and of $W^-=4.9$ eV for the negative surface are in good agreement with the values measured by UV-PEEM at $\approx 10^{-10}$ torr of $W^+ \geq 6.2$ eV for the positive surface and $W^-=4.6$ eV for the negative surface.[16] However, in the cited work the different ionization energies of the two surfaces have been explained with variations in the surface electron affinities associated with surface dipole layers formed by surface adsorbates. Due to the agreement of our calculated ionization energy of the clean surfaces with the measured values, we suggest that the different surface termination itself can explain the observed difference in ionization energy and only the residual deviation from the experiment (a few tenths of an electron volt) is related to the presence of adsorbates on the surface. For both the positive and the negative surfaces,

TABLE III. Ionization energy and surface-induced dipole for the investigated terminations of the positive (left-hand side) and negative (right-hand side) surfaces. A negative dipole value means that the dipole is directed against the spontaneous LN polarization. All values are in electron volt.

Term.	W^+	$\Delta\Phi_{dip}$	Term.	W^-	$\Delta\Phi_{dip}$
-Nb-O	9.7	+1.8		6.3	−0.6
-Nb-O_2	9.9	+2.3	O	9.9	−4.2
-Nb-O_3	10.3	+2.5	O_2	8.7	−3.1
-Nb-O_4	8.8	+1.2	O_3	8.6	−2.8
-Nb-O-Li	5.6	−2.3	Li-	5.6	−0.1
-Nb-O_2-Li	5.7	−2.0	O-Li-	4.9	−0.1
-Nb-O_3-Li	7.5	−0.1	O_2-Li-	5.8	−0.3
-Nb-O_4-Li	7.6	−0.3	O_3-Li-	7.3	−1.7
-Nb-O-Li_2	5.9	−1.6			
-Nb-O_2-Li_2	5.5	−1.5			
-Nb-O_3-Li_2	6.5	−1.4			
-Nb-O_4-Li_2	10.4	+2.1			

the changes in the morphology and composition with respect to the bulk are reflected in a significant decrease in the work function (from 7.5 eV of the bulk termination to 6.5 eV for the positive and from 6.3 to 4.6 eV in the case of the negative surface). However, at least for the positive surface, terminations other than the stable one lead to even lower ionization energies, indicating that lowering the ionization energy cannot be the only driving stabilization mechanism leading to a particular termination. In a further attempt to identify the dominant stabilization mechanisms, we have investigated the surface dipole variations $\Delta\Phi_{dip}$, calculated for each termination with respect to an unrelaxed bulk termination (bulk cut). $\Delta\Phi_{dip}$ has been calculated for each surface as the variation in the potential from the vacuum region through the interface into the bulk. A negative dipole means that the surface dipole is directed against the bulk spontaneous polarization. Due to the choice of our reference, the dipole associated with the stoichiometric terminations (-Nb-O_3-Li for the positive face and Nb for the negative) is relatively small

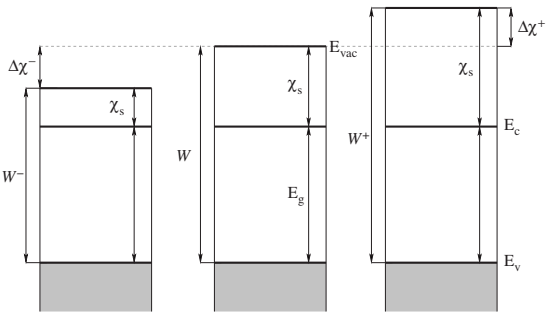

FIG. 11. Schematic energy-band diagram of the (a) negative, (c) positive, and (b) a nonpolar $LiNbO_3$ surface. χ_s and $\Delta\chi$, are the electronic affinity and its variation, E_g is the band gap, E_c, E_v, and E_{vac} are conduction band, valence band, and vacuum energies, *W* is the ionization energy. Superscripts represent the quantities of positive and negative domains.

TABLE IV. Ionization energy and surface-induced dipole for the investigated terminations of the LN *X* cut (left-hand side) and *Y* cut (right-hand side). All values are in electron volt.

Term	W^X	$\Delta\Phi_{dip}$	Term	W^Y	$\Delta\Phi_{dip}$
-Li_3	7.5	−0.5	-Li	6.6	0.7
-Li_6	6.5	−0.7	-LiNb	5.8	0.0
-Li_9	6.4	−0.7	-$LiNb_2$	6.0	0.1
-Li_{12}	6.6	−0.5	-Li_2	5.7	−0.1
-Li_6Nb_6	6.3	−0.9	-Li_2Nb	5.8	0.0
-Nb_3	7.5	0.4	-Li_2Nb_2	6.2	0.4
-Nb_6	6.7	−0.6	-Nb	6.4	0.6
-Nb_9	6.9	−0.4	-Nb_2	6.1	0.3
-Nb_{12}	7.5	0.3	-O_1	7.5	1.6
-O_3	6.2	−1.2	-O_2	7.4	1.5
-O_6	6.2	−1.0	-O_3	7.8	1.9
-O_9	7.7	0.5	-O_4	7.7	2.0
-O_{12}	8.5	1.4	-O_5	6.8	1.0
-O_{15}	8.6	1.5	-O_6	6.8	1.0
-O_{18}	8.2	0.9	-$Li_2Nb_2O_6$	7.9	2.0

and is due only to the relaxation of the geometry. As one would expect, the stable terminations (-Nb-O_3-Li_2 for the positive face and O-Li- for the negative) introduce a surface dipole directed against the spontaneous polarization, thus reducing the total polarization. In this way, the surface charge is reduced and the surface stabilized. However, again other terminations would be even more effective in reducing the polarization surface charge by introducing a surface dipole against the spontaneous polarization so that we have to conclude that the preferred surface is not determined by only one dominant relaxation mechanism but rather by the interplay of many of them. Levchenko and Rappe explain the stability of the preferred positive and negative terminations by passivation of the surface charges by ions.[19]

B. *X* cut

Along the *x* direction, LN can be thought of as a succession of Li_6Nb_6-O_9-O_9 trilayers. In contrast to the *z* direction, the *x* direction is neither polar nor piezoelectric. As the crystal *x* axis is perpendicular to a crystal mirror plane, any charge displacement due to a compression along the *x* axis is mirrored on the other side of the plane and does not gives rise to piezoelectric effects. While reconstructions on the LN *Z* cut have been excluded by RHEED/LEED,[15] we are not aware of corresponding information for the *X* cut and *Y* cut. Still, our computational investigations are restricted to 1×1 surface unit cells. To model the stoichiometric and nonstoichiometric terminations perpendicular to the $[2\bar{1}\bar{1}0]$ direction, we consider as surface layer -Li_6Nb_6-O_{3i}, with $i=1,\ldots,6$ and -Li_{3x} and -Nb_{3y}, with $x=0,\ldots,4$, $y=0,\ldots,4$, as reported in Table IV. Each stoichiometry is then investigated within different starting geometries. We want to remark that our choice of candidate surface terminations does not include all the possible surface stoichiometries but is rather a sampling which allows to scan different configurations. Nevertheless, we think that the main conclusions of our simulation, such as the chemical trends and the surface morphology, will not be affected by other possible stable terminations entering the phase diagram. The resulting phase diagram is shown in Fig. 12. The -Li_{12} termination is the dominant one and is formed under most growth conditions. However, other stable terminations such as -Li_6Nb_6-O_9 and (for very O-rich conditions) -Li_9 can be formed. The stable surface terminations are shown in Fig. 13. The -Li_{12} termination is characterized by the relaxation of an -O_3 layer above the -Li_{12} layer and otherwise a minor ionic relaxation (see Fig. 13 and Table V). The dominance of the -Li_{12} structure confirms that the stability of nonstoichiometric terminations is a general phenomenon of transition-metal-oxide surfaces.[46] Just like in the case of other corundum structured oxides (M_2O_3), which have a structure that closely resembles

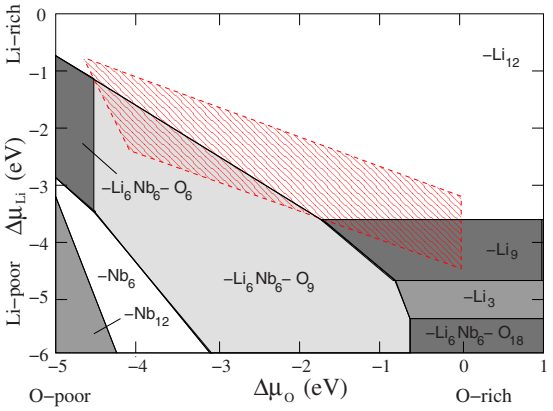

FIG. 12. (Color online) Phase diagram of the LN *X* cut at different growth conditions and in absence of foreign adsorbates. The shaded region indicates the thermodynamically range of the chemical potentials.

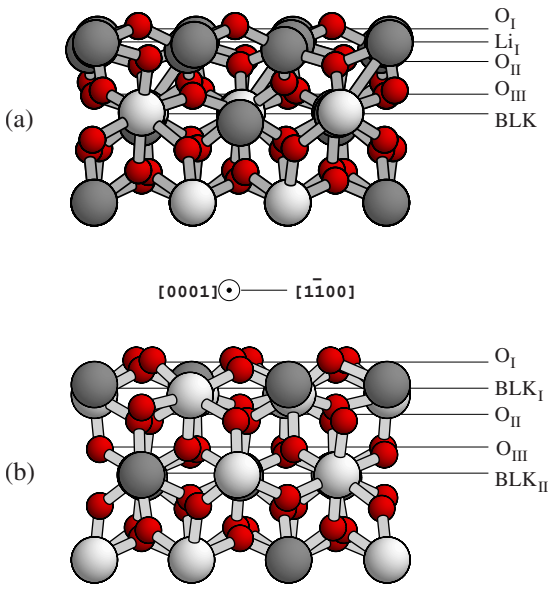

FIG. 13. (Color online) Side view of the dominant (a) -Li_{12} and (b) -Li_6Nb_6-O_9 terminations of the LN *X* face. White atoms are Nb, gray atoms Li, and small atoms O.

TABLE V. Distances between the atomic layers of the stable LN *X* and *Y* surfaces. Corresponding bulk values are reported for comparison, all lengths in angstrom.

	Surf.	Bulk
	X(-Li_{12})	
$d(O_I, O_{II})$	1.06	
$d(O_I, O_{III})$	1.91	
$d(Li_I, O_I)$	0.57	
$d(BLK, O_{III})$	0.85	0.86
	X(-Li_6Nb_6-O_9)	
$d(O_I, BLK_I)$	0.79	0.86
$d(O_I, BLK_{II})$	3.45	3.44
$d(BLK_I, BLK_{II})$	2.65	2.58
$d(O_{II}, O_{III})$	1.04	0.86
	Y	
$d(O_I, Nb_I)$	0.66	
$d(O_I, O_{II})$	1.26	
$d(O_I, O_{III})$	2.03	
$d(O_I, O_{IV})$	2.69	
$d(O_I, BLK_I)$	1.55	1.49

LN with both cationic sites occupied by the same atom type, the metallic termination is the most stable one, as long as no H is present in the environment in contact with the surface.[46] It is known that for the cited oxides, the stable terminations is the one which minimizes the surface work function and the surface dipole moment. For the LN *X* cut, there is not one single termination with both the smallest work function and surface dipole. However, -Li_{12} is among the terminations with the lowest electronic ionization energy (6.6 eV) and has one of the smallest surface dipoles (−0.5 eV), as can be seen in Table IV. Positive dipole values in the table indicate that the dipole points along the *x* direction.

C. *Y* cut

The LN *Y* cut has attracted some interest not only because of its technological importance but also because it shows a puzzling surface charge, which is not expected for a nonpolar material cut.[25] Along the *y* axis, LN can be interpreted as a sequence of $Li_2Nb_2O_6$ layers, as shown in Fig. 5. The *y* direction ($[1\bar{1}00]$ or equivalent) is parallel to a crystal mirror plane: Any charge movements due to ionic displacement (compression) is not compensated for and gives rise to piezoelectricity. The *y* axis is therefore nonpolar but piezoelectric. The terminations considered to model the *Y* cut are -O_x, with $x=1,\ldots 6$ and -Li_i-Nb_j, with $i,j=0,1,2$ and all possible combinations, as reported in Table IV. For each of these combinations, different starting geometries have been modeled. In this way, we consider stoichiometric and nonstoichiometric terminations. As in the case of the *X* cut not all the possible terminations are investigated. The dominant termination in the phase diagram of the *Y* cut is the bulk termination -$Li_2Nb_2O_6$, however in case of strongly Li-rich or O-rich growth conditions the surface can become Li terminated or O terminated (see Fig. 14). Assuming the bulk termination to be the dominant one, it seems, at first sight, difficult to explain the observed surface charge. However, the bulk termination (represented in Fig. 15) cannot be simply considered as a truncated bulk. Indeed, it is characterized by an outward relaxation of two oxygen atoms above the cation layer, which in turn results in the biggest surface dipole (2.0 eV) of all the investigated terminations (see Tables IV and V). As before, positive dipole values in the table indicate that the dipole points in the positive *y* direction, negative values that the dipole points in the negative *y* direction. The pronounced relaxation of the surface atoms with the formation of a strong surface dipole (the LN *Y* cut is piezoelectric) may explain the surface charge observed in these nominally nonpolar cuts.[25]

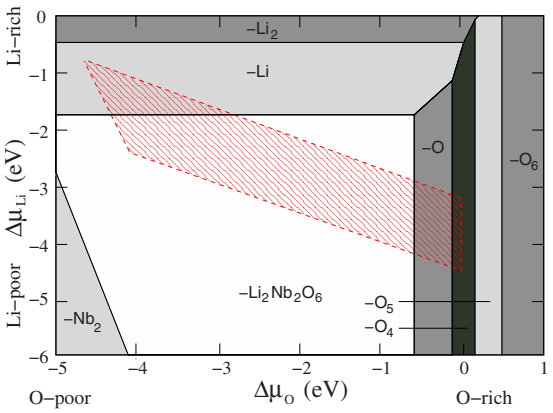

FIG. 14. (Color online) Phase diagram of the LN *Y* cut at different growth conditions and in absence of foreign adsorbates. The unlabeled region represents the stoichiometric termination, i.e., the bulk cut plus a whole $Li_2Nb_2O_6$ layer. The shaded region indicates the thermodynamically allowed range of the chemical potentials.

V. SUMMARY

The surfaces of ferroelectric $LiNbO_3$ usually known as *X* cut, *Y* cut, and *Z* cut have been calculated using density-functional theory. For the *Z* cut, we find a strong influence of

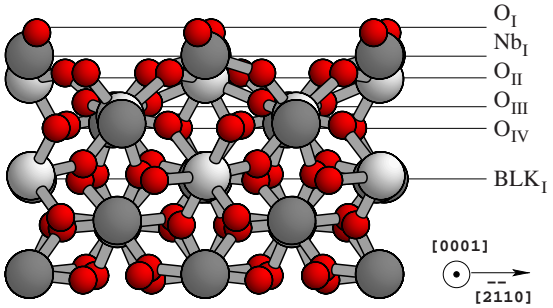

FIG. 15. (Color online) Side view of the stable (-Li_2-Nb_2-O_6 terminated) LN *Y* face at growth conditions. White atoms are Nb, gray atoms Li, and small atoms O.

the spontaneous polarization of the material on the surface structure. The positive z face is found to be -Nb-O_3-Li_2 terminated for all thermodynamically allowed growth conditions and is characterized by an ionization energy of 6.5 eV. The negative z face is O-Li- terminated (under strongly O-rich conditions it becomes O_2 or O_3 terminated) and is characterized by an ionization energy of 4.9 eV. While one of the topmost Li atoms of the positive surface sinks into the lower-lying O layer, no change in the atomic layer ordering occurs at the negative surfaces. The atomic relaxation of both faces is rather moderate and involves only the uppermost atoms. The formation of the z faces does not alter the insulating nature of LN. The nonpolar LN x face is dominated by the -Li_{12} termination, confirming the generally observed trend for a metal termination of corundum structured metal oxide surfaces. The stable termination is characterized by an ionization energy of 6.6 eV. The LN y face is -$Li_2Nb_2O_6$ terminated for almost all growth conditions. Even if this termination has a stoichiometric composition, it cannot be considered as a truncated bulk. It is in fact characterized by a pronounced outward relaxation of the topmost oxygen atoms. Due to the piezoelectricity of the LN y axis, this has a major effect in the charge distribution. The piezoelectric effect together with the strong surface dipole introduced by the stable termination explains the surface charge observed on the Y cut .

ACKNOWLEDGMENTS

We thank Wolfgang Sohler for suggesting this work and many helpful discussions. The calculations were done using grants of computer time from the Paderborn Center for Parallel Computing (PC^2) and the Höchstleistungs-Rechenzentrum Stuttgart (HLRS). The Deutsche Forschungsgemeinschaft is acknowledged for financial support.

*simone.sanna@uni-paderborn.de

[1] Y. Xu, *Ferroelectric Materials and Their Applications* (Elsevier, Amsterdam, 1991).
[2] Y. S. Kuzminov, *Lithium Niobate Crystals* (Cambridge International Science, Cambridge, 1999).
[3] R. S. Weis and T. K. Gaylord, Appl. Phys. A **37**, 191 (1985).
[4] T. Volk and M. Wöhlecke, *Lithium Niobate: Defects, Photorefraction and Ferroelectric Switching* (Springer, Berlin, 2008).
[5] S. Grilli, P. Ferraro, P. De Natale, B. Tiribilli, and M. Vassalli, Appl. Phys. Lett. **87**, 233106 (2005).
[6] Y. Yun and E. I. Altman, J. Am. Chem. Soc. **129**, 15684 (2007).
[7] W. A. Doolittle, G. Namkoong, A. G. Carver, and A. S. Brown, Solid-State Electron. **47**, 2143 (2003).
[8] G. Namkoong, K. Lee, S. M. Madison, W. Henderson, S. E. Ralph, and W. A. Doolittle, Appl. Phys. Lett. **87**, 171107 (2005).
[9] K. Lee, G. Namkoong, W. A. Doolittle, M. Losurdo, G. Bruno, and D. H. Jundt, J. Vac. Sci. Technol. B **24**, 2093 (2006).
[10] Y. Tsuchiya, A. Kobayashi, J. Ohta, H. Fujioka, and M. Oshima, Phys. Status Solidi A **202**, R145 (2005).
[11] Y. Tsuchiya, M. Oshima, A. Kobayashi, J. Ohta, and H. Fujioka, J. Vac. Sci. Technol. A **24**, 2021 (2006).
[12] A. Ougazzaden, T. Moudakir, T. Aggerstam, G. Orsal, J. P. Salvestrini, S. Gautier, and A. A. Sirenko, Phys. Status Solidi C **5**, 1565 (2008).
[13] S. Sanna and W. G. Schmidt, Appl. Surf. Sci. **256**, 5740 (2010).
[14] D. D. Fong, A. M. Kolpak, J. A. Eastman, S. K. Streiffer, P. H. Fuoss, G. B. Stephenson, C. Thompson, D. M. Kim, K. J. Choi, C. B. Eom, I. Grinberg, and A. M. Rappe, Phys. Rev. Lett. **96**, 127601 (2006).
[15] Y. Yun, M. Li, D. Liao, L. Kampschulte, and E. I. Altman, Surf. Sci. **601**, 4636 (2007).
[16] W. Yang, B. J. Rodriguez, A. Gruverman, and R. J. Nemanic, Appl. Phys. Lett. **85**, 2316 (2004).
[17] G. H. Lee, Opt. Express **10**, 556 (2002).
[18] A. Ye Lushkin, V. B. Nazarenko, K. N. Pilipchak, V. F. Shnyukov, and A. G. Naumovets, J. Phys. D **32**, 22 (1999).
[19] S. V. Levchenko and A. M. Rappe, Phys. Rev. Lett. **100**, 256101 (2008).
[20] S. Sanna and W. G. Schmidt, Phys. Status Solidi C **7**, 145 (2010).
[21] L. Gui, H. Hu, M. Garcia-Granda, and W. Sohler, Opt. Express **17**, 3923 (2009).
[22] S. Solanki, T.-C. Chong, and X. Xu, J. Cryst. Growth **250**, 134 (2003).
[23] A. Räuber, *Chemistry and Physics of Lithium Niobate*, Current Topics in Matial Science Vol. 1, edited by E. Kaldis (North-Holland, Amsterdam, 1978).
[24] T. Jungk, A. Hoffmann, and E. Soergel, Appl. Phys. Lett. **89**, 042901 (2006).
[25] F. Johann, T. Jungk, A. Hoffmann, and E. Soergel (private communication).
[26] P. E. Blöchl, Phys. Rev. B **50**, 17953 (1994).
[27] G. Kresse and J. Furthmüller, Phys. Rev. B **54**, 11169 (1996).
[28] J. P. Perdew and Y. Wang, Phys. Rev. B **33**, 8800 (1986).
[29] W. G. Schmidt, M. Albrecht, S. Wippermann, S. Blankenburg, E. Rauls, F. Fuchs, C. Rödl, J. Furthmüller, and A. Hermann, Phys. Rev. B **77**, 035106 (2008).
[30] J. Neugebauer and M. Scheffler, Phys. Rev. B **46**, 16067 (1992).
[31] L. Bengtsson, Phys. Rev. B **59**, 12301 (1999).
[32] H. J. Monkhorst and J. D. Pack, Phys. Rev. B **13**, 5188 (1976).
[33] G.-X. Qian, R. M. Martin, and D. J. Chadi, Phys. Rev. Lett. **60**, 1962 (1988).
[34] W. G. Schmidt, Appl. Phys. A **65**, 581 (1997).
[35] F. Bechstedt, *Principle of Surface Physics* (Springer, Berlin, 2003).
[36] H. Xu, D. Lee, J. He, S. B. Sinnott, V. Gopalan, V. Dierolf, and S. R. Phillpot, Phys. Rev. B **78**, 174103 (2008).
[37] F. Furche, Phys. Rev. B **64**, 195120 (2001).
[38] Ralph W. G. Wyckoff, *Crystal Structures* (Krieger, Malabar, Florida, 1982), Vol. 1.
[39] B. M. Gatehouse and A. D. Wadsley, Acta Crystallogr. **17**, 1545 (1964).
[40] O. Knacke, O. Kabaschewski, and K. Hesselmann, *Thermo-*

chemical Properties of Inorgnic Substances (Springer Verlag, Berlin, 1991).
[41] M. W. Chase, Jr., J. Phys. Chem. Ref. Data **9**, 1 (1998).
[42] T. Choso, M. Kamada, and K. Tabata, Appl. Surf. Sci. **121-122**, 387 (1997).
[43] K. Tabata, T. Choso, and Y. Nagasawa, Surf. Sci. **408**, 137 (1998).
[44] A. Saito, H. Matsumoto, S. Ohnisi, M. Akai-Kasaya, Y. Kuwahara, and M. Aono, Jpn. J. Appl. Phys. **43**, 2057 (2004).
[45] G. X. Qian, R. M. Martin, and D. J. Chadi, Phys. Rev. B **37**, 1303 (1988).
[46] K. Reuter and M. Scheffler, Phys. Rev. B **65**, 035406 (2001).